AMERICAN SOCIETY FOR MICROBIOLOGY | Journal of Bacteriology

Loss of PodJ in *Agrobacterium tumefaciens* Leads to Ectopic Polar Growth, Branching, and Reduced Cell Division

James C. Anderson-Furgeson, John R. Zupan, Romain Grangeon, Patricia C. Zambryski

Department of Plant and Microbial Biology, University of California, Berkeley, California, USA

ABSTRACT

***Agrobacterium tumefaciens* is a rod-shaped Gram-negative bacterium that elongates by unipolar addition of new cell envelope material. Approaching cell division, the growth pole transitions to a nongrowing old pole, and the division site creates new growth poles in sibling cells. The *A. tumefaciens* homolog of the *Caulobacter crescentus* polar organizing protein PopZ localizes specifically to growth poles. In contrast, the *A. tumefaciens* homolog of the *C. crescentus* polar organelle development protein PodJ localizes to the old pole early in the cell cycle and accumulates at the growth pole as the cell cycle proceeds. FtsA and FtsZ also localize to the growth pole for most of the cell cycle prior to Z-ring formation. To further characterize the function of polar localizing proteins, we created a deletion of *A. tumefaciens podJ* (*podJ*$_{At}$). Δ*podJ*$_{At}$ cells display ectopic growth poles (branching), growth poles that fail to transition to an old pole, and elongated cells that fail to divide. In Δ*podJ*$_{At}$ cells, *A. tumefaciens* PopZ-green fluorescent protein (PopZ$_{At}$-GFP) persists at nontransitioning growth poles postdivision and also localizes to ectopic growth poles, as expected for a growth-pole-specific factor. Even though GFP-PodJ$_{At}$ does not localize to the midcell in the wild type, deletion of *podJ*$_{At}$ impacts localization, stability, and function of Z-rings as assayed by localization of FtsA-GFP and FtsZ-GFP. Z-ring defects are further evidenced by minicell production. Together, these data indicate that PodJ$_{At}$ is a critical factor for polar growth and that Δ*podJ*$_{At}$ cells display a cell division phenotype, likely because the growth pole cannot transition to an old pole.**

IMPORTANCE

How rod-shaped prokaryotes develop and maintain shape is complicated by the fact that at least two distinct species-specific growth modes exist: uniform sidewall insertion of cell envelope material, characterized in model organisms such as *Escherichia coli*, and unipolar growth, which occurs in several alphaproteobacteria, including *Agrobacterium tumefaciens*. Essential components for unipolar growth are largely uncharacterized, and the mechanism constraining growth to one pole of a wild-type cell is unknown. Here, we report that the deletion of a polar development gene, *podJ*$_{At}$, results in cells exhibiting ectopic polar growth, including multiple growth poles and aberrant localization of cell division and polar growth-associated proteins. These data suggest that PodJ$_{At}$ is a critical factor in normal polar growth and impacts cell division in *A. tumefaciens*.

Cell wall synthesis generally occurs in two modes in well-studied Gram-negative rod-shaped bacteria such as *Escherichia coli*. For division, cell wall peptidoglycan synthesis occurs at the midcell, resulting in septation. A protein complex called the divisome is responsible for septal peptidoglycan synthesis. The tubulin homolog FtsZ and the actin-like FtsA are essential for divisome structure and function. In model rod-shaped bacteria, the localization of these proteins at the midcell ensures equal division into two daughter cells (1). Additionally, rod-shaped bacteria must elongate prior to the subsequent division. This second mode of cell wall synthesis involves uniform insertion of new peptidoglycan throughout the length of the sidewall of the rod cell and is accomplished by a protein complex called the elongase (2–4).

Members of the alphaproteobacterial order *Rhizobiales*, such as *Agrobacterium tumefaciens*, undergo cell division at the midcell and encode most of the known divisome components (5). However, these bacteria produce new peptidoglycan material for elongation in a remarkably different manner involving a single pole of the bacterial cell (6). Peptidoglycan synthesis at the growth pole occurs by a mechanism that maintains rod shape and is similar to the growth mode of *Streptomyces* and *Mycobacterium* species (7–10). Once the *Agrobacterium* cell has elongated sufficiently, cell wall synthesis machinery ceases activity at the growth pole and begins activity at the division site (5, 11). New growth poles in daughter cells arise at the poles created by division (11, 12). Finally, these organisms lack homologs of most of the elongase components, found in well-studied bacteria such as *Escherichia coli* or *Caulobacter crescentus* (5).

Unipolar growth in *A. tumefaciens* necessitates the development and maintenance of polar asymmetry by spatial and temporal regulation of the machinery involved in the creation of new cell envelope material. Remarkably, *A. tumefaciens* cell division proteins are possibly involved in polar growth, as hallmark cell division proteins such as FtsA and FtsZ localize to the growth pole during polar growth and subsequently localize to the midcell during division (5, 12, 13). As the cell approaches division, elongation at the growth pole stops and this pole transitions to an old pole (5,

Received 4 March 2016 **Accepted** 26 April 2016

Accepted manuscript posted online 2 May 2016

Citation Anderson-Furgeson JC, Zupan JR, Grangeon R, Zambryski PC. 2016. Loss of PodJ in *Agrobacterium tumefaciens* leads to ectopic polar growth, branching, and reduced cell division. J Bacteriol 198:1883–1891. doi:10.1128/JB.00198-16.

Editor: P. de Boer, Case Western Reserve University School of Medicine

Address correspondence to Patricia C. Zambryski, zambrysk@berkeley.edu.

J.C.A.-F. and J.R.Z. contributed equally to this work.

Supplemental material for this article may be found at http://dx.doi.org/10.1128/JB.00198-16.

11, 12). Therefore, polar growth must be negatively regulated during the switch to becoming an old pole.

To further understand *A. tumefaciens* polar growth and to identify molecular players in pole identity, we are studying the localization patterns of proteins known to play roles in polar development in other alphaproteobacteria (14, 15). Though some alphaproteobacteria, such as *C. crescentus*, do not grow through unipolar growth, polar asymmetry and development are a noted feature of their cell cycles. Several *C. crescentus* gene products are asymmetrically localized in a cell-cycle-dependent fashion to affect these developmental processes. One polar localizing protein, *C. crescentus* PopZ ($PopZ_{Cc}$), is required for development of the flagellated pole into the stalked pole and for chromosome segregation (14, 16–18). Another gene product, PodJCc, functions in development of polar organelles such as pili, flagella, and the adhesive holdfast (15) and is involved in the polar localization of cell cycle regulators such as PleC (15, 19). In *Sinorhizobium meliloti* (RM1021), which grows through unipolar elongation like *A. tumefaciens* (11), deletion of *S. meliloti* (RM1021)-specific *podJ1* alters cell morphology, flagellar motility, cell envelope composition, and localization of cell-cycle-regulating factors such as DivK (20).

Putative homologs of $PodJ_{Cc}$ and $PopZ_{Cc}$ were recently characterized in *A. tumefaciens* (21). While *A. tumefaciens* PopZ ($PopZ_{At}$) localizes exclusively to growing poles, green fluorescent protein (GFP)-$PodJ_{At}$ localizes predominantly to the old pole and accumulates at the growth pole late in the cell cycle as the growth pole transitions into an old pole (21); thus, we suggested that $PodJ_{At}$ may determine old pole identity in *A. tumefaciens*. To further test the role of *A. tumefaciens*-specific $PodJ_{At}$ in orchestrating polar development, we created an *A. tumefaciens podJ* ($podJ_{At}$) deletion. Indeed, deletion of this gene resulted in ectopic growth poles and cell division defects that dramatically altered cell morphology. Notably, $PopZ_{At}$ localized to ectopic poles in the $podJ_{At}$ deletion and the cell division proteins FtsA and FtsZ localized to division sites that failed to septate. Together, these data suggest that $PodJ_{At}$ is a critical factor in normal polar growth and that its absence impacts cell division.

MATERIALS AND METHODS

Strains and cell growth conditions. Strains used in this study are listed in Table S1 in the supplemental material. *A. tumefaciens* strain C58 containing pTiC58 (22) was transformed with the relevant plasmids and grown in LB medium at 28°C. LB medium with low salt (LBLS medium) and peptone-yeast extract (PYE) media were prepared as described previously (20). For time-lapse experiments, overnight cultures were diluted to 10^8 cells/ml and grown for 4 to 5 h before imaging. Lactose-inducible expression was achieved by adding 2.5 mM IPTG (isopropyl-β-D-thiogalactopyranoside) to cultures.

Flagellar motility assay. Flagellar motility assays were performed on semisolid LB medium with 0.3% agar plates. Small colonies grown on regular LB agar plates were picked with sterile thin P200 pipette tips. The pipette tips were submerged into the semisolid agar and imaged after 2 days of incubation at 28°C.

Spot titer growth assay. Cells were grown overnight in LB at 28°C, centrifuged, resuspended at 10^8 cells/ml in the different media, and then grown for 4 to 5 h at 28°C. Cell suspensions were then diluted in a series of 10-fold dilutions in the same growth medium. Ten microliters of cell suspension for each dilution was spotted on plates. Plates were incubated for 2 days at 28°C and imaged.

Molecular cloning and strain construction. Standard molecular cloning techniques were used to construct strains (23). The Δ$podJ_{At}$ strain was constructed by transforming C58 with pJZ237, selecting for a single crossover into the genome by growing on carbenicillin, and then selecting for a second recombination by growth on sucrose. pJZ237 (see Table S1 in the supplemental material) is derived from a vector created by cloning the *Bacillus subtilis sacB* gene conferring sucrose sensitivity (24) into a SacI site in the Stratagene pBluescript II SK vector, which cannot replicate in *A. tumefaciens*. The deletion of $podJ_{At}$ was verified by PCR and sequencing.

Time-lapse microscopy. B04A microfluidic plates were used with the CellASIC Onix microfluidic system. Plates were flushed with LB with appropriate antibiotics and inducer for 30 min at 4 lb/in^2. Cells (100 μl at 3×10^9 cells/ml) were loaded into the microfluidics chamber from a suspension at 3×10^9 cells/ml and perfused with LB with appropriate antibiotics and inducer. Cells were imaged in a chamber with a ceiling height of 0.7 μm for 3 to 4 h. Cells were then imaged on an Applied Precision DeltaVision deconvolution fluorescence microscope. Images were processed using Fiji software.

Fluorescence microscopy. Cells were grown in LB overnight, diluted in LB with IPTG, and grown for 4 h. Slides with agarose pads (1% agarose in phosphate-buffered saline [PBS], pH 7) were prepared. Cells were resuspended in FM4-64 for 5 min to stain cell membranes, applied to agarose pads, covered with a coverslip, and imaged on the DeltaVision microscope.

Scanning electron microscopy (SEM). Cells were fixed in 2% glutaraldehyde in 0.1 M sodium cacodylate buffer, rinsed with sodium cacodylate buffer, postfixed in 1% osmium tetroxide in sodium cacodylate buffer, dehydrated to 100% ethanol, critical point dried, mounted on gold stubs, and imaged using a Hitachi S-5000 scanning electron microscope.

Cell labeling. Approximately 9×10^8 cells were fixed in ice-cold methanol for 10 min at −20°C in 5 μg/ml FM4-64FX (Life Technologies). Two to 3 μl of cells was pipetted onto poly-L-lysine-coated coverslips and air dried. Coverslips were washed 3 times with PBS (pH 7), and 1 μg/ml 4′,6-diamidino-2-phenylindole (DAPI) was added to cells to label nucleic acids. Texas Red succinimidyl ester (TRSE) labeling was performed as described previously (5).

RESULTS

We recently characterized the localization of *A. tumefaciens* wild-type (WT) GFP-$PodJ_{At}$ and $PopZ_{At}$-GFP. While $PopZ_{At}$ remains a growth-pole-specific marker throughout the cell cycle, GFP-$PodJ_{At}$ localizes to the old pole and then also to the growth pole during the later stages of polar elongation, potentially marking the transition of the growth pole into an old pole just prior to cell division (21). The localization patterns of GFP-$PodJ_{At}$ and $PopZ_{At}$-GFP as well as the cell division proteins FtsA-GFP and FtsZ-GFP are summarized in Fig. S1 in the supplemental material. To provide further insight into the requirement for the dynamic localization of GFP-$PodJ_{At}$, we monitored cell cycle progression and the localization of polar development proteins in a $podJ_{At}$ deletion strain (Δ$podJ_{At}$).

$podJ_{At}$ (Atu0499) is located in a genomic context more similar to *S. meliloti podJ* ($podJ_{Sm}$) in strain SM11 than *C. crescentus podJ* ($podJ_{Cc}$) (Fig. 1), as might be expected for two members of the *Rhizobiales*. Δ$podJ_{At}$ was created through allelic exchange resulting in a markerless deletion of the Atu0499 open reading frame and the short hypothetical Atu0500 open reading frame that overlaps the 5′ end of Atu0499. Transcription of Atu0500, however, was not detected in microarray data, indicating that it is not likely expressed (25). Deletion of $podJ_{At}$ was verified by PCR amplification of the Atu0499 locus and flanking regions from genomic DNA and sequencing of the PCR product.

Deletion of $podJ_{At}$ results in major growth abnormalities. Deletion of $podJ_{At}$ causes morphological aberrations compared to WT *A. tumefaciens*. Δ$podJ_{At}$ cells stained with the membrane dye FM4-64 (Fig. 2A and B) are elongated, often with multiple con-

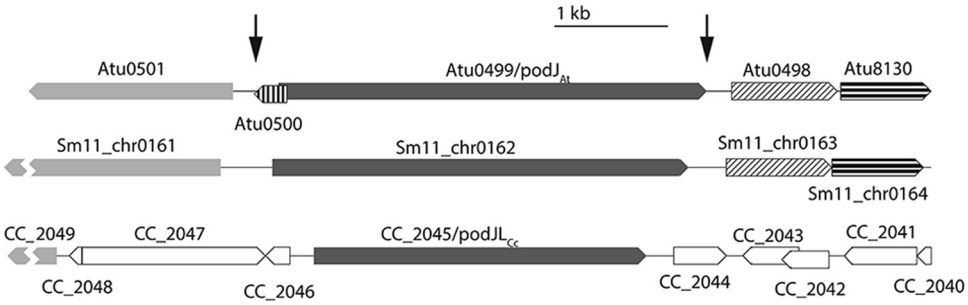

FIG 1 *podJ* genomic contexts in *A. tumefaciens*, *S. meliloti*, and *C. crescentus*. Atu numbers refer to *A. tumefaciens* strain C58 locus tags, Sm11_chr numbers refer to *S. meliloti* strain SM11 locus tags, and CC_ numbers refer to *C. crescentus* CB15N locus tags. Open reading frames that are similarly shaded or patterned are reciprocal best BLAST hits. Open reading frames that are white are not homologous to any other open reading frame shown. Breaks in *S. meliloti* and *C. crescentus* open reading frames reflect open reading frames that extend beyond the area shown. The Δ*podJ*$_{At}$ strain was created using allelic exchange to remove both *podJ*$_{At}$ and the small overlapping reading frame Atu0500 in the region between the arrows.

strictions. In WT cells, FM4-64 predominantly stains the old nongrowing poles (12), as summarized in Fig. S1 in the supplemental material. Notably, many Δ*podJ*$_{At}$ cells are branched or swollen. Bent cells and small spherical Δ*podJ*$_{At}$ cells are also observed. The frequencies of morphological deviations from rod shape observed in Δ*podJ*$_{At}$ cells compared to WT cells are summarized in Fig. 3. In scanning electron microscopy (SEM) images of Δ*podJ*$_{At}$ cells, constrictions are more numerous than in lower-resolution light micrographs and cells with multiple branches are also better resolved (Fig. 2C and D). A gallery of SEM images of Δ*podJ*$_{At}$ cells (see Fig. S2 in the supplemental material) shows additional examples of branched and multiply constricted cells as well as cells with tapered poles.

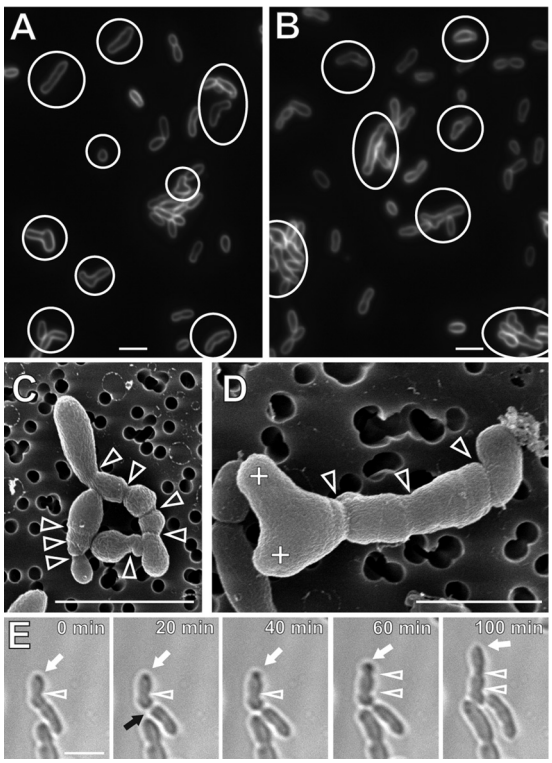

FIG 2 Δ*podJ*$_{At}$ cells are elongated, branched, multiply constricted, and swollen and show ectopic polar growth. (A and B) FM4-64-labeled Δ*podJ*$_{At}$ cells. Cells with morphological deviations from rod shape, such as cells with multiple constrictions, branched cells, swollen cells, and bent cells, are indicated with circles or ovals. (C and D) SEM images of Δ*podJ*$_{At}$ cells displaying deviations from rod-shape morphology, including elongated cells, branched cells, and cells with multiple constrictions. Arrowheads denote cell constrictions (variations in cell width). Plus signs indicate branch tips. (E) Time-lapse images of Δ*podJ*$_{At}$ cells undergoing polar growth (white arrow) and a division event (black arrow). White arrowheads denote cell constrictions. Bars, 3 μm.

We then used time-lapse light microscopy to follow the morphological deviations from rod shape that occur during the Δ*podJ*$_{At}$ cell cycle. Identification of growth poles in time-lapse images of *A. tumefaciens* is based on cell morphology. In WT *A. tumefaciens*, the parent cell compartment, with an old, nongrowing pole at its end, is consistently wider than the new cell compartment, with a growing pole at its end. As the cell approaches division, the growth pole widens to attain the same width as the old, nongrowing pole. The difference in widths between mother and daughter cell compartments can be used to distinguish the growing daughter cell end of the cell from the nongrowing end (5, 11).

Identification of growth poles based on the width of cell compartments in time-lapse microscopy is also supported by pulse-chase labeling of cell envelope material in Δ*podJ*$_{At}$ and WT strains (see Fig. S3 in the supplemental material). Texas Red succinimidyl ester (TRSE) labels outer membrane proteins in *A. tumefaciens* (5, 11). In a chase period after cell labeling, new unlabeled cell enve-

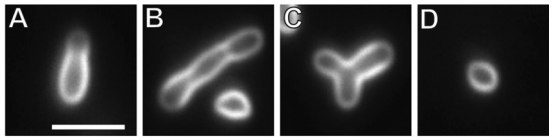

	WT	Δ*podJ*$_{At}$	Δ*podJ*$_{At}$+ GFP-PodJ$_{At}$	Δ*podJ*$_{At}$+ PodJ$_{At}$
A: Rod-shaped	96%	60%	87%	93%
B: Multiple constriction/ bent	4%	29%	7%	4%
C: Branched/ swollen	0%	8%	5%	2%
D: Minicell	0%	3%	1%	1%

FIG 3 Frequency of morphological abnormalities in Δ*podJ*$_{At}$ cells. Percentages of WT cells (n = 283), Δ*podJ*$_{At}$ cells (n = 262), Δ*podJ*$_{At}$ cells expressing GFP-PodJ$_{At}$ (n = 340), and Δ*podJ*$_{At}$ cells expressing PodJ$_{At}$ (n = 247) displaying different morphologies are shown below representative images. Bar, 3 μm.

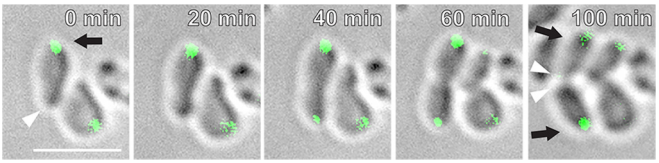

FIG 4 Complementation of Δ*podJ*$_{At}$ with GFP-PodJ$_{At}$ restores cell morphology and dynamic polar localization of GFP-PodJ$_{At}$. In the early stages of the cell cycle (0 to 20 min), GFP-PodJ$_{At}$ localizes as a large focus at the old pole (arrow). Arrowheads indicate the growth pole postdivision at 0 min and future growth poles at 100 min. A small GFP-PodJ$_{At}$ focus develops at the postdivision growth pole at 40 min. Postdivision, GFP-PodJ$_{At}$ localizes as large foci at old poles (100 min, arrows). For simplicity, arrows and arrowheads are shown only in the first and last panels. Bar, 3 μm.

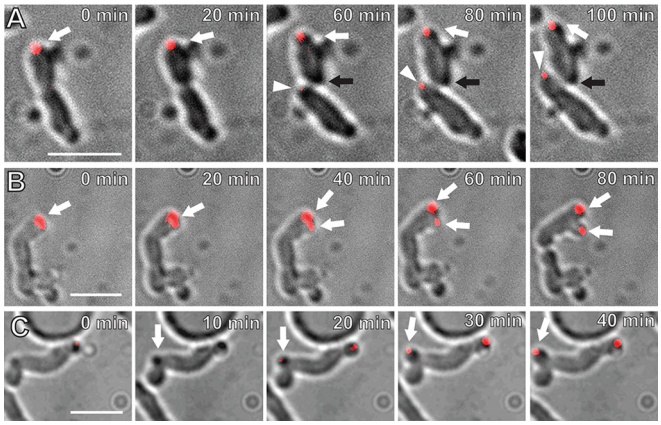

FIG 5 PopZ$_{At}$-GFP localizes to ectopic growth poles in Δ*podJ*$_{At}$ cells. (A) The Δ*podJ*$_{At}$ cell on the top displays a PopZ$_{At}$-GFP focus (red) at a growing pole (white arrow) that continues to grow postdivision. The black arrow indicates a pole produced by division (60 min) that should normally be a growth pole, but it does not grow and does not label with PopZ$_{At}$-GFP. In contrast, the lower sibling cell grows from the site of division, as in the WT (arrowhead), and this new growth pole does label with PopZ$_{At}$-GFP. (B) Δ*podJ*$_{At}$ cell displaying splitting of the growth pole and producing two PopZ$_{At}$-GFP foci (arrows). (C) Δ*podJ*$_{At}$ cell with PopZ$_{At}$-GFP focus at a growth pole emerging from a convex point along the sidewall of the cell (arrow). Bars, 3 μm.

lope material is added to growing Δ*podJ*$_{At}$ cells (see Fig. S3A, 30 to 50 min, and B, 30 to 40 min) and WT cells (see Fig. S3C, 20 to 40 min). All unlabeled new poles are narrower than the labeled, nongrowing poles. Additionally, time-lapse videos clearly indicate polar growth from the (narrower) pole identified as the growth pole (see Videos S1 and S2 in the supplemental material).

Some Δ*podJ*$_{At}$ cells continue to grow from the pole opposite the division site, which normally would be the old nongrowing pole in WT cells (Fig. 2E; see also Video S3 and Fig. S3A, 30 to 50 min, cell on the right, and B, 30 to 40 min, cell on the right, all in the supplemental material). In contrast, WT cells grow from poles derived from a division event (see Fig. S3C, 20 to 40 min, and schematic of WT growth in Fig. S1). Ectopic polar growth (Fig. 2E, white arrow) continues for at least 80 min. This cell also develops two constrictions (Fig. 2E, arrowheads) that normally indicate the site(s) of septum formation; however, no septum formation was observed in this Δ*podJ*$_{At}$ cell.

Though 60% of Δ*podJ*$_{At}$ cells appear morphologically normal in static images (Fig. 3), time-lapse imaging suggests that many of these cells develop altered morphologies during the course of one or two cell cycles. Videos S1 and S2 in the supplemental material show two examples of such cells that begin by apparently normal polar growth and division but then give rise to sibling cells with ectopic growth poles and defects in morphology. Thus, the development of Δ*podJ*$_{At}$ morphological phenotypes is a stochastic process.

As Videos S1 and S2 in the supplemental material better document the Δ*podJ*$_{At}$ phenotype, we next quantified the patterns of growth during time-lapse imaging of 151 Δ*podJ*$_{At}$ cells and 148 WT cells during the cell cycle (see Table S2 in the supplemental material). Division events produced two sibling cells displaying a normal pattern of polar growth in 100% of WT cells and in only 53% of Δ*podJ*$_{At}$ cells. In Δ*podJ*$_{At}$ cells, 37% of cells produced one cell with an ectopic growth pole, 3% gave rise to one normal-growing cell and one nongrowing cell, and 7% gave rise to one ectopic polar-growing cell and one nongrowing cell.

The growth rate of the Δ*podJ*$_{At}$ strain as measured by the optical density of a culture at 600 nm (OD_{600}) in liquid medium was not different from that of the WT (see Fig. S4 in the supplemental material). However, the mean CFU ml^{-1} $OD_{600}{}^{-1}$ was 1.24×10^9 ($n = 6$) for the WT and only 1.09×10^9 ($n = 6$) for the Δ*podJ*$_{At}$ strain. A two-tailed *t* test gave a *P* value of 0.0193, indicating a significant difference in colony-forming abilities between the two strains, potentially due to lower viability of larger or very short Δ*podJ*$_{At}$ cells (see below). Alternatively, the longer and branched cells in Δ*podJ*$_{At}$ may increase their optical density (compared to the WT) while yielding fewer CFU. Thus, in spite of morphological abnormalities, the Δ*podJ*$_{At}$ strain is capable of growth and division.

GFP-PodJ$_{At}$ expression partially complements, and PodJ$_{At}$ expression fully complements, Δ*podJ*$_{At}$ strain growth abnormalities. We tested whether limited expression of GFP-PodJ$_{At}$ or unfused PodJ$_{At}$ under the control of a tightly regulated *lac* promoter on a low-copy-number plasmid (26) could complement Δ*podJ*$_{At}$. A large fraction of Δ*podJ*$_{At}$ cells expressing GFP-PodJ$_{At}$ or PodJ$_{At}$ (not fused to GFP) displayed normal rod-shaped morphology (87% and 93%, respectively), compared to Δ*podJ*$_{At}$ (60%) (Fig. 3). We also monitored 142 Δ*podJ*$_{At}$ cells expressing PodJ$_{At}$ by time-lapse microscopy and found that 97% of the division events were normal (see Table S2 in the supplemental material). It is notable that PodJ$_{At}$ can still function when fused to GFP. Figure 4 and Video S4 in the supplemental material exemplify a cell displaying one growing pole and one nongrowing pole (0 to 20 min). Then, from 20 to 40 min the cell divides, and from 60 to 100 min, the two daughter cells grow from the poles created by the cell division event just as in the WT (11, 12). GFP-PodJ$_{At}$ localized predominantly in larger foci at old poles and to smaller foci in new poles just prior to division (as these poles transition to old poles) as observed in the WT (21).

PopZ$_{At}$ localizes to ectopic poles in Δ*podJ*$_{At}$ cells. During WT septation in *A. tumefaciens*, PopZ$_{At}$-GFP disappears from the growth pole of the parent cell and is observed at the growth poles of the sibling cells immediately after completion of cell division (21) (see Fig. S1 in the supplemental material). However, in Δ*podJ*$_{At}$ cells PopZ$_{At}$-GFP often does not leave the growth pole either just before or after septation (Fig. 5A, $t = 0$ to $t = 60$ min, white arrow; see also Video S5 in the supplemental material), and this pole continues to grow ectopically (Fig. 5A, $t = 80$ to 100 min). We monitored 84 dividing Δ*podJ*$_{At}$ cells expressing PopZ$_{At}$-GFP and found that PopZ$_{At}$-GFP failed to relocalize from the

growth pole after division in 35 (42%) of the dividing cells. In contrast, in all 41 time-lapse videos of WT division events, $PopZ_{At}$-GFP relocalizes to the poles derived from the division site in both sibling cells.

Table S2 in the supplemental material documents that often only one of the two $\Delta podJ_{At}$ sibling cells grows post-cell division. We tested whether $PopZ_{At}$-GFP localization can distinguish growing from nongrowing $\Delta podJ_{At}$ sibling cells. Indeed, Fig. 5A shows that $PopZ_{At}$-GFP fluorescence appears at the site of division in the lower sibling cell that exhibits polar growth. Notably, there is no growth from the division site, and no $PopZ_{At}$-GFP fluorescence, in the upper sibling cell, likely because PopZ did not leave the growth pole.

$PopZ_{At}$-GFP also localizes to multiple ectopic growth poles in different $\Delta podJ_{At}$ cells. In one cell (Fig. 5B; see also Video S6 in the supplemental material), both the growing tip and the $PopZ_{At}$-GFP focus start to broaden at 20 min. Between 40 and 80 min, the growth pole as well as the $PopZ_{At}$-GFP focus splits to form two growth poles, each with a $PopZ_{At}$-GFP focus. In another cell, $PopZ_{At}$-GFP localizes to the existing growth pole as well as the ectopic growth pole emerging from a point along the sidewall of the cell (Fig. 5C, 10 min to 40 min, arrow; also see Video S7 in the supplemental material). These data together support our previous findings that $PopZ_{At}$ identifies the growth pole (21) and further suggest that $PopZ_{At}$ also identifies sites of ectopic growth either at existing growth poles or *de novo* from a sidewall. Branched cells (Fig. 2C and D; see also Fig. S2 in the supplemental material) may reflect the underlying ectopic localization of $PopZ_{At}$ to these sites.

The $\Delta podJ_{At}$ strain is defective in the localization and function of cell division proteins. FtsA-GFP and FtsZ-GFP localize to the growth pole in addition to the Z-ring in WT *A. tumefaciens* (12). In the $\Delta podJ_{At}$ strain, FtsA-GFP localization patterns are more heterogeneous than those in WT cells. Aside from the unipolar, unipolar and midcell, and midcell localization patterns (Fig. 6A to C) seen in the WT, in $\Delta podJ_{At}$ cells FtsA-GFP displays a bipolar pattern (Fig. 6F), polar plus peripheral foci (Fig. 6G), polar cluster localization (Fig. 6H), a midcell plus bipolar pattern (Fig. 6D), and multiple Z-ring localization (Fig. 6E). The percentage of $\Delta podJ_{At}$ cells displaying some form of midcell FtsA-GFP localization, ~42% (Fig. 6B to E), was higher than the percentage of WT cells that had FtsA-GFP midcell localization, 22% (see Fig. 2C in reference 12). Additionally, the percentage of $\Delta podJ_{At}$ cells displaying WT polar FtsA-GFP (Fig. 6A) localization without midcell localization, 36%, was significantly lower than the percentage of WT cells with only polar FtsA-GFP localization, 78% (12).

The lengths of $\Delta podJ_{At}$ cells displaying different types of FtsA-GFP localization (Fig. 6I) were compared to the median lengths of WT cells displaying different FtsA-GFP localization patterns determined previously (12) and are summarized in Table S3 in the supplemental material. In all cases, whether $\Delta podJ_{At}$ cells displayed the WT FtsA-GFP localizations (polar, polar plus midcell, and midcell) or aberrant FtsA-GFP localization patterns specific to $\Delta podJ_{At}$, the cell length distributions tended toward longer $\Delta podJ_{At}$ cells than WT cells.

Localization patterns of FtsZ-GFP in $\Delta podJ_{At}$ cells also were compared to previously published localization frequencies of FtsZ-GFP during different stages of the cell cycle in WT cells (12). The $\Delta podJ_{At}$ strain displayed a higher percentage of cells with uncontracted Z-rings (Fig. 7G) or contracted Z-rings (Fig. 7H) (51% total) versus the WT (6% total) and lower percentages of cells with unipolar (10%) or subpolar (9%) FtsZ-GFP localizations (19% total) versus the WT (57% total) (Fig. 7). FtsZ-GFP localized in multiple Z-rings in 1% of $\Delta podJ_{At}$ cells (Fig. 7I). In the $\Delta podJ_{At}$ strain, FtsZ-GFP localizes in persistent Z-rings that do not result in division and persist for at least 120 min (see Fig. S5, white arrowhead, and Video S8 in the supplemental material); additionally, this cell produces a second Z-ring between 120 min and 140 min. Finally, Z-ring placement can be abnormal; at 60 min, there is a small focus at the top of the cell that becomes a Z-ring (see Fig. S5, $t = 60$ to 100 min) that pinches off a very small spherical "cell" at 120 min.

The multiple "rings" observed via FtsZ-GFP and FtsA-GFP localization may contribute to the partial constriction phenotype

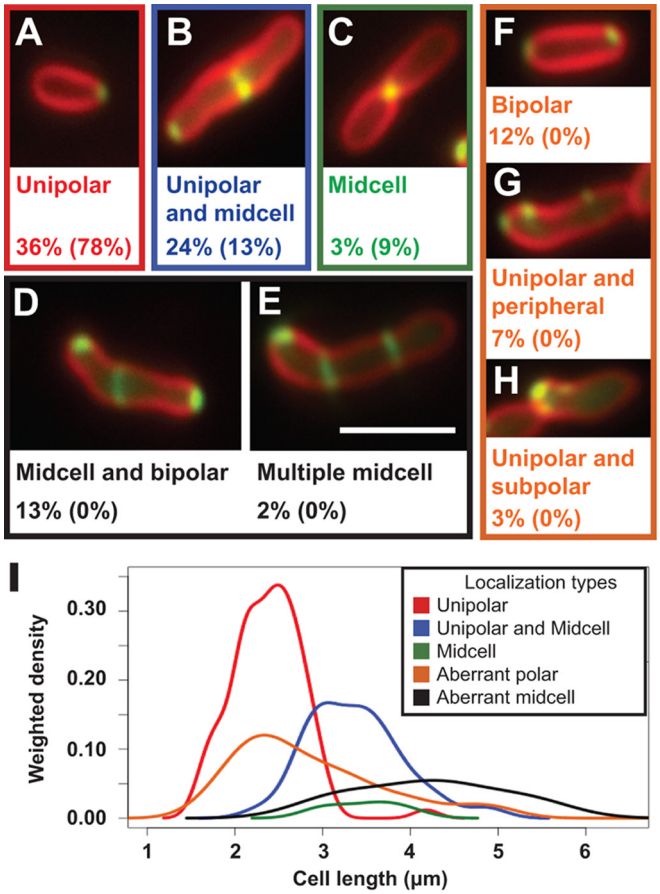

FIG 6 FtsA-GFP localizes in polar foci, lateral foci, and rings in elongated $\Delta podJ_{At}$ cells. $\Delta podJ_{At}$ cells expressing FtsA-GFP stained with FM4-64 display FtsA-GFP patterns seen in WT cells: unipolar (A), unipolar and midcell (B), and midcell (C) localizations. $\Delta podJ_{At}$ cells also display localization patterns of FtsA-GFP not observed in WT cells: bipolar and midcell (D), multiple rings (E), bipolar (F), polar and lateral foci (G), and polar clusters (H). The percentages of $\Delta podJ_{At}$ cells (out of 234 cells total) showing these localization types are shown under representative images, and the percentages of WT cells showing these localization types are shown in parentheses and are from reference 12. Bar, 3 μm. (I) Gaussian kernel density estimates of the distribution of cell lengths of $\Delta podJ_{At}$ cells with different FtsA-GFP localization patterns. Density estimates were weighted by the proportion of cells displaying the different localization types so that the height of the peaks corresponds to the proportion of cells displaying each localization pattern. Colors of density curves correspond to color outlines of representative images of each localization pattern in panels A to H. Bar, 3 μm.

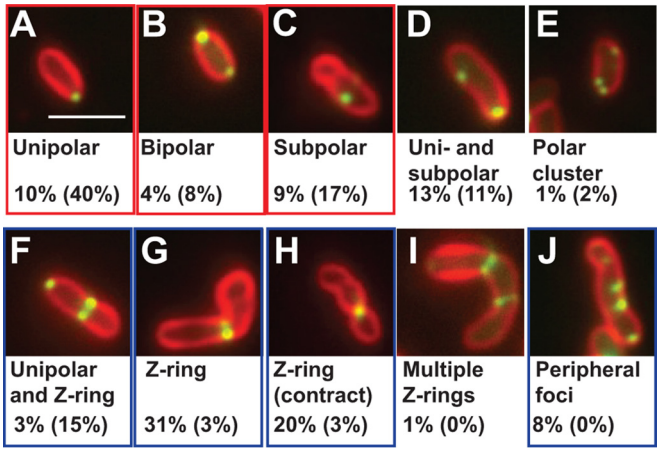

FIG 7 FtsZ-GFP localization in Δ*podJ*$_{At}$ cells. FtsZ-GFP (green) localizes in unipolar (A), bipolar (B), subpolar (C), unipolar and subpolar (D), polar cluster (E), unipolar and Z-ring (F), Z-ring (G), contracting Z-ring (H), multiple-Z-ring (I), and multiple-sidewall-focus (J) patterns in Δ*podJ*$_{At}$ cells. Percentages of Δ*podJ*$_{At}$ cells ($n = 252$) and WT (12) cells (in parentheses) showing different FtsZ-GFP localizations are shown beneath representative images. Localizations seen in notably higher percentages of WT cells than Δ*podJ*$_{At}$ cells are highlighted by red rectangles, and localizations seen in notably higher percentages of Δ*podJ*$_{At}$ cells than WT cells are highlighted by blue rectangles. Bar, 3 μm.

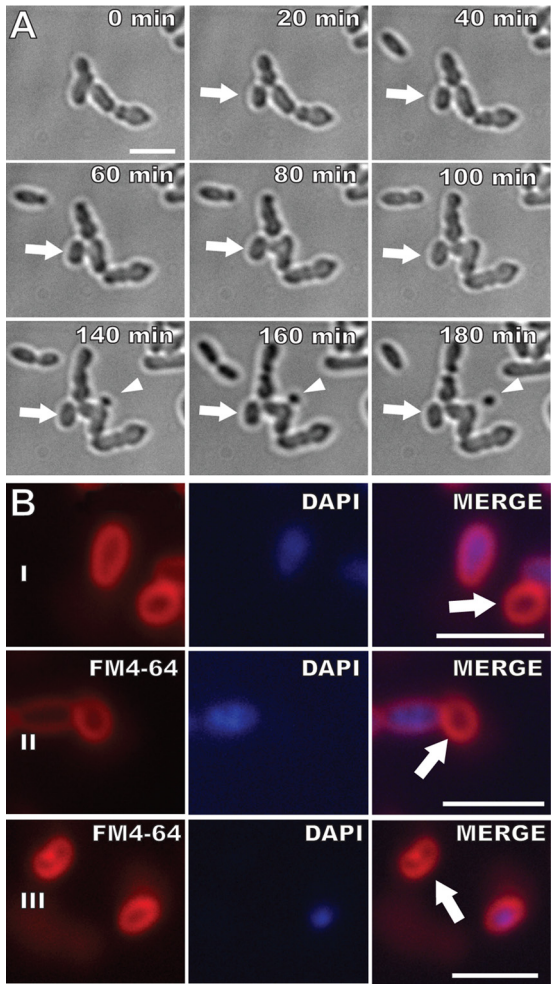

FIG 8 The Δ*podJ*$_{At}$ strain produces nongrowing and small anucleate cells. (A) The arrow indicates a cell that does not grow or divide, and the arrowhead indicates a spherical minicell. (B) FM4-64 and DAPI staining. Some small Δ*podJ*$_{At}$ cells do not stain with DAPI (arrows). Bars, 3 μm.

in many Δ*podJ*$_{At}$ cells with multiple constrictions observed by SEM (Fig. 2C and D; see also Fig. S2 in the supplemental material). That some septal rings (indicated by FtsA- and FtsZ-GFP localization) do not constrict indicates that Δ*podJ*$_{At}$ cells have a defect in division.

The Δ*podJ*$_{At}$ strain displays a division and timing defect resulting in anucleate minicells. Multiple Z-rings and division events producing small cells in Δ*podJ*$_{At}$ cells suggest that the Δ*podJ*$_{At}$ strain displays a division timing or placement defect. Indeed, time-lapse images of Δ*podJ*$_{At}$ cells indicate that division events sometimes produce small cells that do not undergo further growth or division (Fig. 8A; see also Video S9 in the supplemental material). DAPI staining in Δ*podJ*$_{At}$ cells was compared to that in WT (Fig. 8B). Fewer than 1% of WT cells were shorter than 1 μm and did not stain with DAPI. In contrast, 6% of Δ*podJ*$_{At}$ cells were shorter than 1 μm, and none of these cells were stained with DAPI. Thus, the very small Δ*podJ*$_{At}$ cells observed are anucleate and cannot grow. The occurrence of anucleate Δ*podJ*$_{At}$ cells may partially account for the decrease in CFU of Δ*podJ*$_{At}$ in comparison to the WT.

Comparing Δ*podJ*$_{At}$ cells to *S. meliloti* Δ*podJ1*. PodJ was previously studied in a related member of the *Rhizobiales*, *S. meliloti*. The *S. meliloti* Δ*podJ1* strain also displayed morphological defects such as the branching observed here. The Δ*podJ1* strain also exhibited a motility defect and different growth and morphology phenotypes on different media (20). We observed that the Δ*podJ*$_{At}$ strain also has a partial motility defect in comparison to the WT as observed in a soft agar flagellar motility assay (see Fig. S6 in the supplemental material). The Δ*podJ*$_{At}$ flagellar motility phenotype may reflect that deviations from rod shape decrease the efficiency of flagellar motility in the Δ*podJ*$_{At}$ strain. Or, flagellar subunit transcription may be lower as shown for deletion of *podJ1* in *S. meliloti* (20).

S. meliloti Δ*podJ1* was less viable when grown on LB plates with low salt (LBLS) (20); however, growth in LBLS did not impact the viability of the Δ*podJ*$_{At}$ strain (see Fig. S7 in the supplemental material). Growth in PYE medium improved *S. meliloti* Δ*podJ1* morphology and FtsZ-GFP localization phenotypes (20); however, growth in PYE did not impact the viability of the Δ*podJ*$_{At}$ strain (see Fig. S7). A quantitative assessment of hundreds of cells revealed that growth in PYE medium only partially complemented the morphology phenotype of the Δ*podJ*$_{At}$ strain, reducing the frequency of cells with deviations from rod shape compared with that for Δ*podJ*$_{At}$ cells grown in LB (see Table S4); no quantitative studies were performed in the *S. meliloti* Δ*podJ1* study. In contrast to *S. meliloti* Δ*podJ1*, Δ*podJ*$_{At}$ cells grown in PYE continue to display abnormal FtsZ-GFP localization, including peripheral sidewall localization (see Fig. S8A to E) and multiple ring localization (see Fig. S8F), in addition to normal polar and midcell FtsZ-GFP localization (see Fig. S8G and H). WT cells grown in PYE displayed WT FtsZ-GFP localizations (12), including polar and midcell FtsZ-GFP localization (see Fig. S8I and J). The differences between the phenotypes of the *A. tumefaciens* Δ*podJ*$_{At}$ strain and the *S. meliloti* Δ*podJ1* strain suggest that the

details of PodJ activity may be different in these two organisms. Muropeptide analysis indicates that 64% of peptide stems are cross-linked in *A. tumefaciens* peptidoglycan compared to 43% of peptide stems in *S. meliloti* peptidoglycan (11). The high degree of peptidoglycan cross-linking in *A. tumefaciens* may account for the insensitivity of Δ*podJ*$_{At}$ cells to low-salt media.

DISCUSSION

In WT *A. tumefaciens*, GFP-PodJ$_{At}$ continuously localizes to nongrowing old poles. Importantly, GFP-PodJ$_{At}$ also localizes to growth poles later in the cell cycle when such poles must begin to transition into old poles just before cell division (21). Here, in the absence of PodJ$_{At}$ growth poles fail to transition to old, nongrowth poles and ectopic growth poles are initiated; these results support the idea that PodJ$_{At}$ is a critical factor in normal polar growth in *A. tumefaciens*. Further, the aberrant localization of FtsA- and FtsZ-GFP in Δ*podJ*$_{At}$ cells suggests that PodJ$_{At}$ indirectly impacts both the timing and site of Z-ring assembly. Z-ring function also is altered in Δ*podJ*$_{At}$ cells, as Z-rings form but often do not result in septation and production of daughter cells. The alterations from WT morphology in Δ*podJ*$_{At}$ cells can be seen most readily in dynamic time-lapse videos, where initially morphologically normal-looking cells grow and divide and then stochastically give rise to cells with dramatic deviations from rod shape.

In the WT, a growth pole arises at the septal sites in siblings following cell division. The growth pole is active for most of the cell cycle, and then prior to cell division, it transitions to an old pole (see Fig. S1 in the supplemental material). In Δ*podJ*$_{At}$ cells, ectopic growth poles arise in three different contexts. First, some growth poles fail to transition to old poles and, after cell division, continue to elongate. Second, adjacent growth poles are formed when a single growth pole splits into two growth poles; splitting of the growth pole occurs simultaneously with broadening and splitting of the localization of new pole identity factor PopZ$_{At}$-GFP. Third, some growth poles arise apparently *de novo* from the cell sidewall.

How might PodJ$_{At}$ function? The failure of growth poles to transition and the initiation of ectopic growth poles in the absence of PodJ$_{At}$ suggest that PodJ$_{At}$ (directly or indirectly) acts as a negative regulator of polar growth in *A. tumefaciens*. The constant localization of GFP-PodJ$_{At}$ to nongrowing poles in the WT at first glance supports this suggestion (21). Alternatively, PodJ$_{At}$ might act positively to regulate unknown negative regulators of polar growth. In *C. crescentus*, other developmental factors rely on PodJ$_{Cc}$ for proper localization (15, 19, 27). Late in the *A. tumefaciens* cell cycle, GFP-PodJ$_{At}$ localizes to small foci at growth poles (Fig. 4; see also Fig. S1 in the supplemental material) (21), perhaps reflecting a need for a threshold level of PodJ$_{At}$ to allow localization of other factors to begin the growth pole-old pole transition (discussed further below).

Development of branched morphologies in *A. tumefaciens* and related organisms has been described previously (28–32). Now that we know that *A. tumefaciens* grows by polar growth (5, 11, 12), we may better understand these earlier phenotypes. In rod-shaped organisms such as *E. coli*, which elongate by uniform insertion of new cell envelope material throughout the sidewall, mutations that inhibit cell division cause filamentous morphologies due to continued elongation without cell division (33–35). When polar-growing members of the *Rhizobiales* are subject to mutations inhibiting cell division, branching morphologies result instead (31, 36). As PodJ$_{At}$ is a polar localizing factor, we expected its loss to alter polar growth. However, we also observed that defective cell division and abnormal branching occur in its absence, phenotypes observed for treatments designed to affect cell division in the *Rhizobiales* (31, 37). Given that polar growth and cell division must be intimately connected, potentially the defects in cell division and branching in Δ*podJ*$_{At}$ are secondary consequences resulting from its primary defect in polar growth. An equally plausible interpretation is that the cell division defect is the primary phenotype of Δ*podJ*$_{At}$.

The induction of ectopic polar growth in Δ*podJ*$_{At}$ indicates that there are factors that actively promote or organize polar growth. Indeed, PopZ$_{At}$ localizes to the growth pole of young cells and relocalizes to the growth poles of recently divided daughter cells immediately after septation (21). In *C. crescentus*, PopZ$_{Cc}$ is initially localized to the stalked pole, where it anchors the chromosome. In response to chromosome replication, a second PopZ$_{Cc}$ focus forms at the flagellar pole as part of the chromosome segregation mechanism (16, 38). *C. crescentus* PopZ$_{Cc}$ continuously localizes to old poles and temporarily to new poles as they transition to old poles (38, 39). In contrast, the localization of PopZ$_{At}$-GFP exclusively to growth poles in the WT (21) and to all observed types of ectopic growth poles in Δ*podJ*$_{At}$ cells supports the idea that PopZ$_{At}$ is a candidate polar-growth-promoting factor or marks growth poles.

Besides localizing to the Z-ring as expected, *A. tumefaciens* FtsA-GFP and FtsZ-GFP localize to the growth pole in the WT (5, 12, 13). That *A. tumefaciens* FtsZ may play additional roles in cell growth is supported by studies in the related *Rhizobiales* member *S. meliloti*, where overexpression of FtsZ-GFP caused significant morphological deviations from rod shape (31). In the Δ*podJ*$_{At}$ strain, FtsA-GFP localized in bipolar, subpolar, and peripheral foci, as well as extra Z-rings, patterns not observed in the WT. In the Δ*podJ*$_{At}$ strain, there were significantly fewer FtsA-GFP and FtsZ-GFP foci at the growth poles, and the intensity of polar localization was weaker than that in the WT; thus, abnormalities in polar growth due to the loss of one factor likely impact the localization of other polar localizing factors such as FtsA and FtsZ. A greater proportion of Δ*podJ*$_{At}$ cells than WT cells display Z-ring FtsZ-GFP and FtsA-GFP localization. SEM of Δ*podJ*$_{At}$ cells revealed that many cells displayed multiple shallow constrictions and very few tight constrictions that would be expected for septation. Thus, Δ*podJ*$_{At}$ cells initiate Z-rings readily, but such rings are defective or slowed in contraction and division.

We propose that the cause of the division defect in Δ*podJ*$_{At}$ cells is the failure of PodJ$_{At}$ to direct the transition of the growth pole to an old pole. This hypothesis is supported by our observation that the new pole-localizing factor, PopZ$_{At}$, fails to leave the growth pole in Δ*podJ*$_{At}$ cells. In the WT, PopZ$_{At}$ leaves the growth pole and reappears in both sibling cells at the postseptal sites (21). To enable immediate and equal localization in the two siblings, PopZ$_{At}$ likely arrives at the septum just prior to septation, possibly playing a late cell cycle role in Z-ring function. Our earlier time-lapse studies could not distinguish whether PopZ$_{At}$ migrates or is degraded and then resynthesized and targeted to new growth poles (21). The results here suggest that PopZ$_{At}$ migrates to the septum in WT cells.

Alternatively, PodJ$_{At}$ may have an indirect effect on cell division via its potential requirement for the polar localization and function of additional cell cycle regulators. In *C. crescentus*, PodJ$_{Cc}$

is part of a complex network of proteins, including $PleC_{Cc}$, that activates the master cell cycle regulator CtrA specifically in the nascent swarmer cell compartment and newborn swarmer cell (40). Indeed, in *S. meliloti*, PodJ1 is suggested to play a critical role in $PleC_{Sm}$ signaling, and $PleC_{Sm}$ is essential for cell viability and may play a role in cell division (20). By analogy, $PodJ_{At}$ may influence the localization or activity of components of the cell division and development regulatory pathway, for example, PleC (Atu0982) or DivK (Atu1296) (41). Additionally, $PodJ_{At}$ is longer (1,248 amino acids [aa]) than $PodJ_{Cc}$ (974 aa) and may have additional functions. Note that the two proteins are only 23% identical but both contain a large cytoplasmic domain with numerous coiled-coil regions that may mediate interactions with other polar factors.

Polar development factors in the alphaproteobacteria can have distinct roles in both polar development and proper cell division. In *C. crescentus*, TipN is critical in positioning new-pole structures such as flagella and exerts an influence on cell division by interacting with ParA at the new pole during chromosome segregation (42). Similarly, $PodJ_{At}$ may impact polar growth and cell division independently.

Relatively little is known about the factors that regulate polar growth, and many questions remain to be addressed (43). Regarding $PodJ_{At}$, does it function as a negative or positive regulator of polar growth? What factors keep $PodJ_{At}$ forever at old poles? How is polar growth machinery disassembled at the growth pole? Does $PodJ_{At}$ interact with $PopZ_{At}$? Does the arrival of $PodJ_{At}$ directly signal the departure of $PopZ_{At}$? Do *A. tumefaciens* homologs of cell cycle regulators depend on $PodJ_{At}$ for polar localization and play a role in the transition of a growth pole into an old pole? Understanding the regulation of cellular asymmetry that mediates unipolar growth in *A. tumefaciens* will likely uncover new paradigms for bacterial morphogenesis.

ACKNOWLEDGMENTS

We thank Steven Ruzin and Denise Schichnes of the Biological Imaging Facility, UC Berkeley, for assistance with fluorescence microscopy. We thank Gwangwei Min at the Electron Microscopy Laboratory at UC Berkeley for assistance with scanning electron microscopy. We thank Clarence Kado of University of California, Davis, for the NT1REB strain.

FUNDING INFORMATION

Research was supported by National Science Foundation grant MCB-0923840 (to P.C.Z.). J.C.A.-F. also thanks the William Caroll Smith Fellowship Fund for support. The funders had no role in study design, data collection and interpretation, or the decision to submit the work for publication.

REFERENCES

1. **den Blaauwen T, de Pedro MA, Nguyen-Distèche M, Ayala JA.** 2008. Morphogenesis of rod-shaped sacculi. FEMS Microbiol Rev **32:**321–344. http://dx.doi.org/10.1111/j.1574-6976.2007.00090.x.
2. **van Teeffelen S, Wang S, Furchtgott L, Huang KC, Wingreen NS, Shaevitz JW, Gitai Z.** 2011. The bacterial actin MreB rotates, and rotation depends on cell-wall assembly. Proc Natl Acad Sci U S A **108:**15822–15827. http://dx.doi.org/10.1073/pnas.1108999108.
3. **Garner EC, Bernard R, Wang W, Zhuang X, Rudner DZ, Mitchison T.** 2011. Coupled, circumferential motions of the cell wall synthesis machinery and MreB filaments in *B. subtilis*. Science **333:**222–225. http://dx.doi.org/10.1126/science.1203285.
4. **Domínguez-Escobar J, Chastanet A, Crevenna AH, Fromion V, Wedlich-Söldner R, Carballido-López R.** 2011. Processive movement of MreB-associated cell wall biosynthetic complexes in bacteria. Science **333:**225–228. http://dx.doi.org/10.1126/science.1203466.
5. **Cameron TA, Anderson-Furgeson J, Zupan JR, Zik JJ, Zambryski PC.** 2014. Peptidoglycan synthesis machinery in *Agrobacterium tumefaciens* during unipolar growth and cell division. mBio **5:**e01219–14. http://dx.doi.org/10.1128/mBio.01219-14.
6. **Brown PJB, Kysela DT, Brun YV.** 2011. Polarity and the diversity of growth mechanisms in bacteria. Semin Cell Dev Biol **22:**790–798. http://dx.doi.org/10.1016/j.semcdb.2011.06.006.
7. **Braña AF, Manzanal M-B, Hardisson C.** 1982. Mode of cell wall growth of *Streptomyces antibioticus*. FEMS Microbiol Lett **13:**231–235.
8. **Miguélez EM, Martín C, Manzanal MB, Hardisson C.** 1992. Growth and morphogenesis in *Streptomyces*. FEMS Microbiol Lett **100:**351–359.
9. **Meniche X, Otten R, Siegrist MS, Baer CE, Murphy KC, Bertozzi CR, Sassetti CM.** 2014. Subpolar addition of new cell wall is directed by DivIVA in mycobacteria. Proc Natl Acad Sci U S A **111:**E3243–E3251. http://dx.doi.org/10.1073/pnas.1402158111.
10. **Thanky NR, Young DB, Robertson BD.** 2007. Unusual features of the cell cycle in mycobacteria: polar-restricted growth and the snapping-model of cell division. Tuberculosis **87:**231–236. http://dx.doi.org/10.1016/j.tube.2006.10.004.
11. **Brown PJB, de Pedro MA, Kysela DT, Van der Henst C, Kim J, De Bolle X, Fuqua C, Brun YV.** 2012. Polar growth in the alphaproteobacterial order Rhizobiales. Proc Natl Acad Sci U S A **109:**1697–1701. http://dx.doi.org/10.1073/pnas.1114476109.
12. **Zupan JR, Cameron TA, Anderson-Furgeson J, Zambryski PC.** 2013. Dynamic FtsA and FtsZ localization and outer membrane alterations during polar growth and cell division in *Agrobacterium tumefaciens*. Proc Natl Acad Sci U S A **110:**9060–9065. http://dx.doi.org/10.1073/pnas.1307241110.
13. **Ma X, Sun Q, Wang R, Singh G, Jonietz EL, Margolin W.** 1997. Interactions between heterologous FtsA and FtsZ proteins at the FtsZ ring. J Bacteriol **179:**6788–6797.
14. **Laloux G, Jacobs-Wagner C.** 2013. Spatiotemporal control of PopZ localization through cell cycle-coupled multimerization. J Cell Biol **201:**827–841. http://dx.doi.org/10.1083/jcb.201303036.
15. **Viollier PH, Sternheim N, Shapiro L.** 2002. Identification of a localization factor for the polar positioning of bacterial structural and regulatory proteins. Proc Natl Acad Sci U S A **99:**13831–13836. http://dx.doi.org/10.1073/pnas.182411999.
16. **Bowman GR, Perez AM, Ptacin JL, Ighodaro E, Folta-Stogniew E, Comolli LR, Shapiro L.** 2013. Oligomerization and higher-order assembly contribute to sub-cellular localization of a bacterial scaffold. Mol Microbiol **90:**776–795. http://dx.doi.org/10.1111/mmi.12398.
17. **Laloux G, Jacobs-Wagner C.** 2014. How do bacteria localize proteins to the cell pole? J Cell Sci **127:**11–19. http://dx.doi.org/10.1242/jcs.138628.
18. **Ptacin JL, Gahlmann A, Bowman GR, Perez AM, von Diezmann AR, Eckart MR, Moerner WE, Shapiro L.** 2014. Bacterial scaffold directs pole-specific centromere segregation. Proc Natl Acad Sci U S A **111:**E2046–E2055. http://dx.doi.org/10.1073/pnas.1405188111.
19. **Hinz AJ, Larson DE, Smith CS, Brun YV.** 2003. The *Caulobacter crescentus* polar organelle development protein PodJ is differentially localized and is required for polar targeting of the PleC development regulator. Mol Microbiol **47:**929–941. http://dx.doi.org/10.1046/j.1365-2958.2003.03349.x.
20. **Fields AT, Navarrete CS, Zare AZ, Huang Z, Mostafavi M, Lewis JC, Rezaeihaghighi Y, Brezler BJ, Ray S, Rizzacasa AL, Barnett MJ, Long SR, Chen EJ, Chen JC.** 2012. The conserved polarity factor PodJ1 impacts multiple cell envelope-associated functions in *Sinorhizobium meliloti*. Mol Microbiol **84:**892–920. http://dx.doi.org/10.1111/j.1365-2958.2012.08064.x.
21. **Grangeon R, Zupan JR, Anderson-Furgeson J, Zambryski PC.** 2015. PopZ identifies the new pole, and PodJ identifies the old pole during polar growth in *Agrobacterium tumefaciens*. Proc Natl Acad Sci U S A **112:**11666–11671. http://dx.doi.org/10.1073/pnas.1515544112.
22. **Montoya AL, Chilton MD, Gordon MP, Sciaky D, Nester EW.** 1977. Octopine and nopaline metabolism in *Agrobacterium tumefaciens* and crown gall tumor cells: role of plasmid genes. J Bacteriol **129:**101–107.
23. **Sambrook J, Fritsch EF, Maniatis T.** 1989. Molecular cloning: a laboratory manual, 2nd ed. Cold Spring Harbor Laboratory Press, Cold Spring Harbor, NY.
24. **Blomfield IC, Vaughn V, Rest RF, Eisenstein BI.** 1991. Allelic exchange in *Escherichia coli* using the *Bacillus subtilis sacB* gene and a temperature-sensitive pSC101 replicon. Mol Microbiol **5:**1447–1457. http://dx.doi.org/10.1111/j.1365-2958.1991.tb00791.x.

25. **Klüsener S, Hacker S, Tsai Y-L, Bandow JE, Gust R, Lai E-M, Narberhaus F.** 2010. Proteomic and transcriptomic characterization of a virulence-deficient phosphatidylcholine-negative *Agrobacterium tumefaciens* mutant. Mol Genet Genomics **283:**575–589. http://dx.doi.org/10.1007/s00438-010-0542-7.
26. **Khan SR, Gaines J, Roop RM, Farrand SK.** 2008. Broad-host-range expression vectors with tightly regulated promoters and their use to examine the influence of TraR and TraM expression on Ti plasmid quorum sensing. Appl Environ Microbiol **74:**5053–5062. http://dx.doi.org/10.1128/AEM.01098-08.
27. **Crymes WB, Zhang D, Ely B.** 1999. Regulation of *podJ* expression during the *Caulobacter crescentus* cell cycle. J Bacteriol **181:**3967–3973.
28. **Fujiwara T, Fukui S.** 1972. Isolation of morphological mutants of *Agrobacterium tumefaciens*. J Bacteriol **110:**743–746.
29. **Su S, Stephens BB, Alexandre G, Farrand SK.** 2006. Lon protease of the alpha-proteobacterium *Agrobacterium tumefaciens* is required for normal growth, cellular morphology and full virulence. Microbiology **152:**1197–1207. http://dx.doi.org/10.1099/mic.0.28657-0.
30. **Kahng LS, Shapiro L.** 2001. The CcrM DNA methyltransferase of *Agrobacterium tumefaciens* is essential, and its activity is cell cycle regulated. J Bacteriol **183:**3065–3075. http://dx.doi.org/10.1128/JB.183.10.3065-3075.2001.
31. **Latch JN, Margolin W.** 1997. Generation of buds, swellings, and branches instead of filaments after blocking the cell cycle of *Rhizobium meliloti*. J Bacteriol **179:**2373–2381.
32. **Fujiwara T, Fukui S.** 1974. Unidirectional growth and branch formation of a morphological mutant, *Agrobacterium tumefaciens*. J Bacteriol **120:**583–589.
33. **Dai K, Lutkenhaus J.** 1991. *ftsZ* is an essential cell division gene in *Escherichia coli*. J Bacteriol **173:**3500–3506.
34. **de Boer PA, Crossley RE, Rothfield LI.** 1989. A division inhibitor and a topological specificity factor coded for by the minicell locus determine proper placement of the division septum in *E. coli*. Cell **56:**641–649. http://dx.doi.org/10.1016/0092-8674(89)90586-2.
35. **Bi E, Lutkenhaus J.** 1993. Cell-division inhibitors SulA and MinCD prevent formation of the Ftsz ring. J Bacteriol **175:**1118–1125.
36. **Cheng J, Sibley CD, Zaheer R, Finan TM.** 2007. A Sinorhizobium meliloti minE mutant has an altered morphology and exhibits defects in legume symbiosis. Microbiology **153:**375–387. http://dx.doi.org/10.1099/mic.0.2006/001362-0.
37. **Fujiwara T, Fukui S.** 1974. Effect of D-alanine and mitomycin-C on cell morphology of *Agrobacterium tumefaciens*. J Gen Appl Microbiol **20:**345–349. http://dx.doi.org/10.2323/jgam.20.345.
38. **Bowman GR, Comolli LR, Zhu J, Eckart M, Koenig M, Downing KH, Moerner WE, Earnest T, Shapiro L.** 2008. A polymeric protein anchors the chromosomal origin/ParB complex at a bacterial cell pole. Cell **134:**945–955. http://dx.doi.org/10.1016/j.cell.2008.07.015.
39. **Ebersbach G, Briegel A, Jensen GJ, Jacobs-Wagner C.** 2008. A self-associating protein critical for chromosome attachment, division, and polar organization in *Caulobacter*. Cell **134:**956–968. http://dx.doi.org/10.1016/j.cell.2008.07.016.
40. **Curtis PD, Brun YV.** 2010. Getting in the loop: regulation of development in *Caulobacter crescentus*. Microbiol Mol Biol Rev **74:**13–41. http://dx.doi.org/10.1128/MMBR.00040-09.
41. **Kim J, Heindl JE, Fuqua C.** 2013. Coordination of division and development influences complex multicellular behavior in *Agrobacterium tumefaciens*. PLoS One **8:**e56682. http://dx.doi.org/10.1371/journal.pone.0056682.
42. **Schofield WB, Lim HC, Jacobs-Wagner C.** 2010. Cell cycle coordination and regulation of bacterial chromosome segregation dynamics by polarly localized proteins. EMBO J **29:**3068–3081. http://dx.doi.org/10.1038/emboj.2010.207.
43. **Cameron TA, Zupan JR, Zambryski PC.** 2015. The essential features and modes of bacterial polar growth. Trends Microbiol **23:**347–353. http://dx.doi.org/10.1016/j.tim.2015.01.003.